ChemComm

COMMUNICATION

View Article Online
View Journal | View Issue

Cite this: *Chem. Commun.*, 2022, **58**, 8073

Received 5th May 2022,
Accepted 20th June 2022

DOI: 10.1039/d2cc02555h

rsc.li/chemcomm

Catalytic machinery in motion: controlling catalysis *via* speed†

Emad Elramadi, ‡ Amit Ghosh,‡ Isa Valiyev, Pronay Kumar Biswas, Thomas Paululat and Michael Schmittel *

Three 3-component copper(I)-based slider-on-deck systems served as catalysts for a click reaction showing a higher catalytic activity with increasing sliding speed. Upon addition of brake stones, the motion of the resulting 4-component machinery was slowed and eventually stopped (on the NMR time scale) with the effect that catalysis was reduced or obstructed.

One of the prerequisites of life is adaptive regulation in living organisms, *e.g.*, the up or down modulation of enzymatic activity inside the cell by multiple control variables.[1] Contrastingly, the activity in manmade catalytic machinery[2] so far is mostly regulated by binary (photo)chemical inputs leading to ON–OFF[3] or UP–DOWN[4,5] regulation. To reach deeper cybernetic control,[6] regulation by more than one input is desirable.[7]

Previously, we have presented catalytic rotors and sliders where the catalytic activity was correlated with the motional speed.[8,9] The faster the motion, the higher was the catalytic activity, however, this could only be shown by comparing different machinery. Herein, this correlation will be confirmed using single catalytic machinery with a reversibly changeable speed controlling the catalytic activity. For multistep toggling of the speed an external input will be applied capitalizing on coordination and constitutional dynamic chemistry (**CDC**).

In detail, the slider-on-deck systems $[Cu_3(\mathbf{1})(\mathbf{2})]^{3+}$ were prepared through self-sorting[10] from the tris-shielded phenanthroline deck **1** and one of three bipeds, the bis-lutidine **2a**, the bis-picoline **2b**[10] or the bis-pyridine biped **2c**[11] in presence of copper(I) ions (Fig. 1). The temporarily free Cu^+ center in the slider-on-deck was expected to catalyse a 1,3-dipolar cycloaddition *via* click chemistry.[12] Based on the architecture of the slider-on-deck, it was conjectured that added 2-pyridine carboxaldehyde (**3**) would bind at the free Cu^+-loaded phenanthroline[13] affording $[Cu_3(\mathbf{1})(\mathbf{2})(\mathbf{3})]^{3+}$. Further addition of 8-aminoquinoline (**4**) was supposed to lead to a reaction with **3** affording the terpyridine-analogue **5**,[14] the latter being expected to form a strong HETTAP[15]-type complex. Due to the different binding affinity of **3** and **5**, the dynamics of the biped in $[Cu_3(\mathbf{1})(\mathbf{2a–c})(\mathbf{3}\text{ or }\mathbf{5})]^{3+}$ should be modulated affecting catalysis.

Firstly, both deck **1** and ligands **2a, b** and **c** were synthesised by following analogous procedures. 2-Pyridine carboxaldehyde (**3**) and 8-amino quinoline (**4**) were commercially available.

When **1**, **2**, and copper(I) ions were mixed at rt in a ratio of 1 : 1 : 3 using CD_2Cl_2 as solvent, the slider-on-deck $[Cu_3(\mathbf{1})(\mathbf{2})]^{3+}$ formed both immediately and quantitatively. It was fully characterized by ^{1}H NMR, ^{1}H–^{1}H COSY NMR, DOSY and mass spectroscopy. As anticipated, it showed a single set of signals for deck **1** and an upfield shift for the proton g-H signal of $[Cu_3(\mathbf{1})]^{3+}$ (Fig. 2) from 7.02 to 6.86, 6.87 and 7.03 ppm in **SIa**, **SIb** and **SIc**, respectively. In contrast, the proton signal 4-H showed a downfield shift from 8.84 to 8.87, 8.87 and 8.89 ppm in **SIa**, **SIb** and **SIc**, respectively. Upon binding of the lutidine units of **2a** to the copper(I) phenanthroline stations the proton signals of b′-H shifted upfield by $\Delta\delta$ = 0.07 ppm. In case of bis-picoline biped **2b**, the proton signals of d′, b′ and c′-H showed equally upfield shifts from 7.20, 7.27 and 8.50 ppm to 7.10, 7.17 and 7.54, respectively. Similarly, the signal groups of b′ and a′-H of bis-pyridine biped **2c** shifted strongly upfield from 7.41 & 8.60 to 7.14 & 6.55 ppm, as shown in Fig. 2.

To determine the sliding speed, the slider-on-deck assemblies $[Cu_3(\mathbf{1})(\mathbf{2})]^{3+}$ were studied by variable temperature (VT) ^{1}H NMR spectroscopy (see ESI,† Fig. S54–S63). In case of **SIa** = $[Cu_3(\mathbf{1})(\mathbf{2a})]^{3+}$, the g-H proton peak of the deck showed coalescence at *ca.* −20 °C, whereas at −40 °C the signal split into two peaks at 6.78 and 6.73 ppm (ratio 2 : 1). The signal at 6.78 ppm was assigned to the lutidine-coordinated copper(I) phenanthroline, whereas the one at 6.73 ppm was attributed to the free copper-loaded phenanthroline. The exchange frequency in $[Cu_3(\mathbf{1})(\mathbf{2a})]^{3+}$ was determined as k_{298} = 2.4 kHz and

Center of Micro and Nanochemistry and (Bio)Technology, Organische Chemie I & II, Universität Siegen, Adolf-Reichwein-Str. 2, D-57068, Siegen, Germany.
E-mail: schmittel@chemie.uni-siegen.de; Tel: +49(0) 2717404356

† Electronic supplementary information (ESI) available: Experimental procedures, characterisation, VT-NMR, spectral data. See DOI: https://doi.org/10.1039/d2cc02555h

‡ Emad Elramadi and Amit Ghosh contributed equally

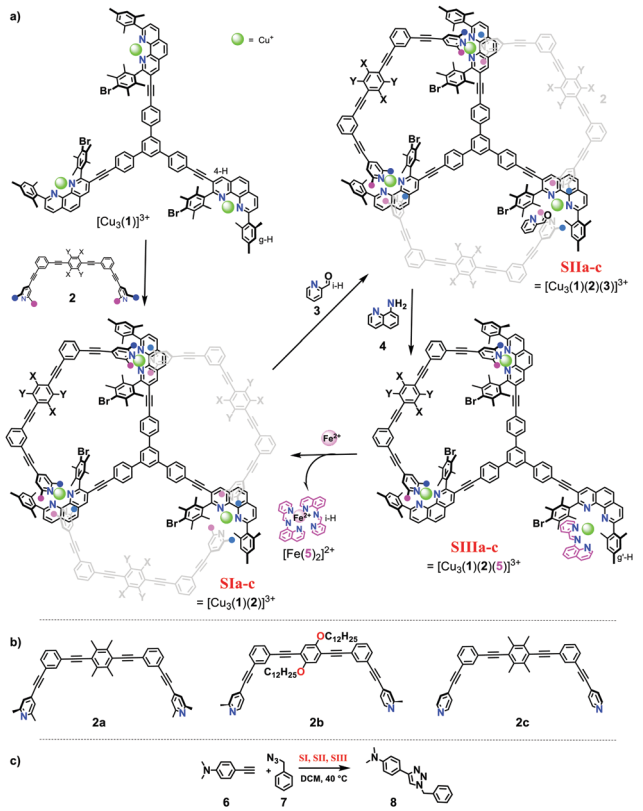

Fig. 1 (a) A three-component slider-on-deck that is modulated upon addition of external stimuli (grey: biped in motion). (b) Molecular structure of biped **2a–c**. (c) Model reaction catalysed by slider-on-deck systems.

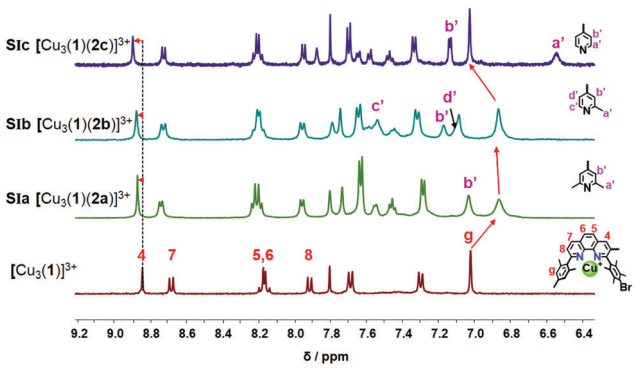

Fig. 2 Comparison of partial ^{1}H NMR spectra (CD_2Cl_2, 500 MHz, 298 K) of copper loaded deck $[Cu_3(\mathbf{1})]^{3+}$, **SIa**: $[Cu_3(\mathbf{1})(\mathbf{2a})]^{3+}$, **SIb**: $[Cu_3(\mathbf{1})(\mathbf{2b})]^{3+}$, **SIc**: $[Cu_3(\mathbf{1})(\mathbf{2c})]^{3+}$. For assignment, partial structures of **1** & **2a–c** are given.

the corresponding free activation energy as $\Delta G^{\ddagger}_{298}$ = 53.7 kJ mol^{-1}. Similarly, the exchange frequency of $[Cu_3(\mathbf{1})(\mathbf{2b})]^{3+}$ was determined to k_{298} = 20 kHz and the corresponding free activation energy as $\Delta G^{\ddagger}_{298}$ = 48.2 kJ mol^{-1}.[10] Finally, the VT ^{1}H NMR spectrum of $[Cu_3(\mathbf{1})(\mathbf{2c})]^{3+}$ showed a singlet for the signal of g-H, which at −70 °C split into two signals at a ratio 2 : 1 at 6.95 and 6.98 ppm. The exchange frequency was determined as k_{298} = 42 kHz and the corresponding free activation energy $\Delta G^{\ddagger}_{298}$ = 46.6 kJ mol^{-1}.

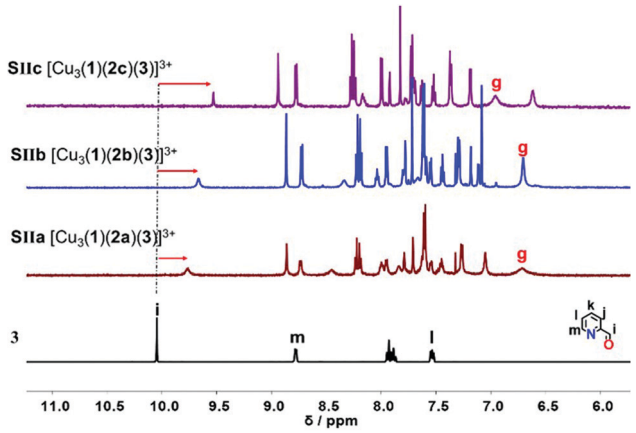

Fig. 3 Comparison of partial ^{1}HNMR spectra (CD_2Cl_2, 600 MHz, 298 K) of ligand **3**, **SIIa** = $[Cu_3(\mathbf{1})(\mathbf{2a})(\mathbf{3})]^{3+}$, **SIIb** = $[Cu_3(\mathbf{1})(\mathbf{2b})(\mathbf{3})]^{3+}$, **SIIc** = $[Cu_3(\mathbf{1})(\mathbf{2c})(\mathbf{3})]^{3+}$.

The binding of the pyridine head groups in bipeds **2a–c** to deck **1** should vary as reflected by the association constants of pyridine, picoline and lutidine to $[Cu(phenAr_2)]^+$ that are $\log K_{py}$ = 3.20,[16] $\log K_{pic}$ = 3.43,[17] and $\log K_{lu}$ = 4.50.[18] As expected, the sliding frequency declined with increasing binding affinity.

Upon addition of one equivalent of 2-pyridine carboxaldehyde (**3**) to a solution of $[Cu_3(\mathbf{1})(\mathbf{2})]^{3+}$ at rt, the four-component assembly $[Cu_3(\mathbf{1})(\mathbf{2})(\mathbf{3})]^{3+}$ formed instantly. A colour change from light yellow to deep red was noticed being characteristic for the complex motif $[Cu(PhenAr_2)(\mathbf{3})]^+$. Furthermore, in the ^{1}H NMR, it showed only one set of signals for deck **1**. The g-H proton peak in $[Cu_3(\mathbf{1})(\mathbf{2a})(\mathbf{3})]^{3+}$, $[Cu_3(\mathbf{1})(\mathbf{2b})(\mathbf{3})]^{3+}$ and $[Cu_3(\mathbf{1})(\mathbf{2c})(\mathbf{3})]^{3+}$ was broadened and shifted upfield to 6.80, 6.74, and 6.84 ppm, respectively, alike the aldehyde proton i-H signal that was shifted from 10.04 to 9.76, 9.65, and 9.61 ppm, respectively, as shown in Fig. 3.

In the VT ^{1}H NMR of $[Cu_3(\mathbf{1})(\mathbf{2a})(\mathbf{3})]^{3+}$, the signal of proton g-H coalesced at 10 °C and as the temperature reached −10 to −20 °C it split into two distinct signals at 6.78 and 6.54 ppm (ratio 2 : 1). The first signal was assigned to the lutidine-coordinated copper(I) phenanthroline while the signal at 6.54 ppm was attributed to the 2-pyridine carboxaldehyde-coordinated copper(I) phenanthroline unit. The exchange frequency and the free activation energy were determined to k_{298} = 1.6 kHz and of $\Delta G^{\ddagger}_{298}$ = 55.2 kJ mol^{-1}. Thus, it shows slower sliding than $[Cu_3(\mathbf{1})(\mathbf{2a})]^{3+}$. The VT ^{1}H NMR of $[Cu_3(\mathbf{1})(\mathbf{2b})(\mathbf{3})]^{3+}$ revealed splitting of the signal of proton 4-H at −25 °C into two distinct signals at 8.88 and 8.84 ppm (ratio 2 : 1) at −35 °C. The exchange frequency and the free activation energy were determined to k_{298} = 11 kHz and $\Delta G^{\ddagger}_{298}$ = 49.8 kJ mol^{-1}. In the VT ^{1}H NMR of $[Cu_3(\mathbf{1})(\mathbf{2c})(\mathbf{3})]^{3+}$ the signal of proton 4-H coalesced at −35 °C and was split into two distinct signals at 8.89 and 8.84 ppm (ratio 2 : 1) at −50 °C. The analysis provided an exchange frequency k_{298} = 26 kHz and $\Delta G^{\ddagger}_{298}$ = 47.8 kJ mol^{-1} (see ESI,† Fig. S54–S63).

To investigate the catalytic activity of the three nanodevices $[Cu_3(\mathbf{1})(\mathbf{2a–c})]^{3+}$ in a click reaction, the reactants **6** and **7**

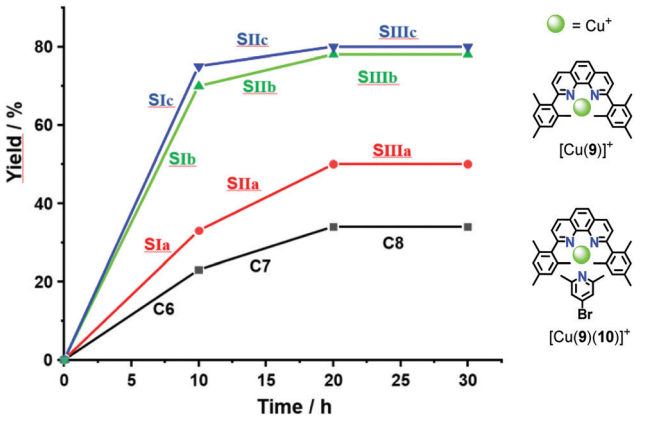

Fig. 4 Yield of the click product **8** (from **6** and **7**, each c = 1.20 × 10^{-2} M) in states **SIa–c**, **SIIa–c** (each c = 40.0 × 10^{-6} M) and with model complexes **C6** = $[Cu(\mathbf{9})]^+$, **C7** = $[Cu(\mathbf{9})(\mathbf{10})]^+$ (c = 1.20 × 10^{-3} M) after 10 h at 40 °C for each state.

(1 : 30 : 30) (the full mixture is denoted as States **SIa–c**) were mixed in CD_2Cl_2. After 10 h at 40 °C, the ^{1}H NMR indicated a yield of 33%, 70% and 75% of **8**, respectively. After addition of consumed amounts of **6** and **7** as well as of 2-pyridine carboxaldehyde (**3**) to form $[Cu_3(\mathbf{1})(\mathbf{2a–c})(\mathbf{3})]^{3+}$, setting up **SIIa–c**, the solution was heated again for 10 h at 40 °C. The yield of **8** increased by 13%, 8% and 5%. No yield was found in **SIIIa–c** (Fig. 4 and Table 1).

For deeper insight, the catalytic activity of the slider-on-deck needed to be assessed relative to that of model complexes. For instance, the yield of **SIa** (33% of **8**) may be compared with that of **C6** = $[Cu(\mathbf{9})]^+ + 2 \times [Cu(\mathbf{9})(\mathbf{10})]^+$ (23% of **8**) representing all binding sites in **SIa**. Analogously, the yield of **SIIa** (13% of **8**) may be compared with that of **C7** = $2 \times [Cu(\mathbf{9})(\mathbf{10})]^+ + [Cu(\mathbf{3})(\mathbf{9})]^+$ (11% of **8**) this mixture embodying all binding sites in **SIIa**. In both cases, the catalytic activity of the slider-on-deck is higher. These examples suggest that both (a) thermodynamic and (b) kinetic aspects influence the catalytic activity: (a) dissociation of the complexes frees some of the copper(I) centres for catalysis. (b) On top, there are dynamic effects of motion in any slider-on-deck that liberate copper(I) centres by moving the biped foot to another location on the deck. The sliding motion may not only kick out the added ligand **3** in **SIIa–c**,[7] but also bound product **8** in both **SIa–c** and **SIIa–c**.

As the sliding frequency increases in **SIa–c**, the click yield is higher. For instance, **SIc** furnished 75% of **8**, while **SIb** afforded 70% and **SIa** only 33%. Clearly, the faster the sliding, the higher is the copper(I) availability due to kicking out the product and the higher is the catalytic activity. Yet, the binding strength of the biped ($N_{pic} > N_{py}$) also plays a role in freeing **8** as otherwise the yield difference would be larger for **SIb** vs **SIc**.

On the other hand, considering the sliding speed, the situation looks opposite for **SIIa–c**. The slowest slider-on-deck in **SIIa** generated 13% of **8**, while the faster ones in **SIIb** and **SIIc** afforded less, *i.e.*, 8% and 5%, respectively. Using ^{1}H NMR, we determined how much of **3** was liberated into solution in each of the slider-on-deck systems $[Cu_3(\mathbf{1})(\mathbf{2a})(\mathbf{3})]^{3+}$ (Fig. S74–75, Table S3 and S4, ESI,†). Accordingly, aldehyde **3** is being kicked out to a higher extent by the lutidine feet in $[Cu_3(\mathbf{1})(\mathbf{2a})(\mathbf{3})]^{3+}$ (47% of free **3**) than in $[Cu_3(\mathbf{1})(\mathbf{2b})(\mathbf{3})]^{3+}$ (26% of free **3**) and in $[Cu_3(\mathbf{1})(\mathbf{2c})(\mathbf{3})]^{3+}$ (19% of free **3**). Here, the liberation seems to follow a thermodynamic motif: the stronger the binding of the biped the more of the brake may be liberated which is equivalent to temporarily freeing a copper(I) site for catalysis (Fig. 5).

Finally, we chose catalyst $[Cu_3(\mathbf{1})(\mathbf{2a})(\mathbf{3})]^{3+}$ to evaluate its behaviour upon addition of one equiv. of 8-aminoquinoline (**4**), which caused the *in situ* formation of $[Cu_3(\mathbf{1})(\mathbf{2a})(\mathbf{5})]^{3+}$ *via* imine bond formation. In the ^{1}H NMR, the signal of mesityl protons g:g′:g″-H showed three distinctive signals (ratio 4 : 1 : 1) (ESI,† Fig. S36). The larger peak at 6.80 ppm was attributed to the lutidine-coordinated copper phenanthroline moiety and the smaller signals at 6.33 and 6.18 ppm were assigned to the mesityl group of the copper phenanthroline bound to imine **5**. The finding of two different mesityl g-H proton signals in one of the phenanthroline sites already indicated that the complex was not dynamic on the NMR timescale, a conclusion additionally supported by the EXSY analysis, because there was no cross peaks between g, g′-H proton signals (ESI,† Fig. S64).

Addition of 0.5 equiv. of iron(II) ions with respect to deck **1** enticed the imine away from the copper(I) phenanthroline into formation of the highly stable hexa-coordinated complex $[Fe(\mathbf{5})_2]^{2+}$. As a result, $[Cu_3(\mathbf{1})(\mathbf{2a})]^{3+}$ was regained and its dynamic motion reset.

Catalysis along **SIa** → **SIIa** → **SIIIa** → **SIa** (10 h at 40 °C) was first evaluated with deck **1**, biped **2a** and copper(I) ions (1 : 1 : 3)

Table 1 Experimental exchange frequency k at 25 °C and activation parameters of **SIa–c** and **SIIa–c** and the yield of the click transformation **6** + **7** → **8** (after 10 h at 40 °C)

State	Slider-on-deck	k_{298} (kHz)	$\Delta G^{\ddagger}_{298}$ (kJ mol^{-1})	Yield of **8** (%)
SIa	$[Cu_3(\mathbf{1})(\mathbf{2a})]^{3+}$	2.4	53.7	33
SIb	$[Cu_3(\mathbf{1})(\mathbf{2b})]^{3+}$	20	48.2	70
SIc	$[Cu_3(\mathbf{1})(\mathbf{2c})]^{3+}$	42	46.6	75
SIIa	$[Cu_3(\mathbf{1})(\mathbf{2a})(\mathbf{3})]^{3+}$	1.6	55.2	13
SIIb	$[Cu_3(\mathbf{1})(\mathbf{2b})(\mathbf{3})]^{3+}$	11	49.8	8
SIIc	$[Cu_3(\mathbf{1})(\mathbf{2c})(\mathbf{3})]^{3+}$	26	47.8	5

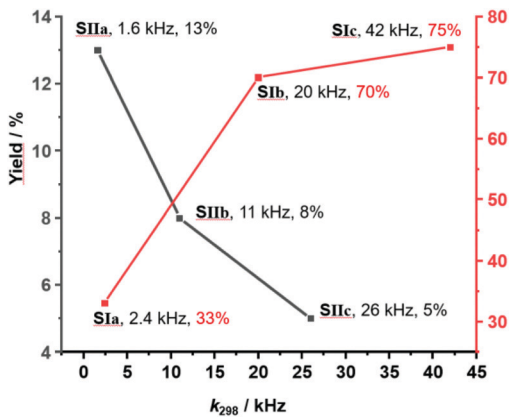

Fig. 5 Representation of yield % *vs.* exchange frequency of **SIa–c** and **SIIa–c** showing an inverse relation.

Table 2 Yield of product formed *vs.* sliding frequency of **SIa**, **SIIa** and **SIIIa**

State	k_{298} (kHz)	Yield ^{1st}cycle (%)	Yield ^{2nd}cycle (%)
SIa = $[Cu_3(\mathbf{1})(\mathbf{2a})]^{3+}$	2.4	33	30
SIIa = $[Cu_3(\mathbf{1})(\mathbf{2a})(\mathbf{3})]^{3+}$	1.6	13	10
SIIIa = $[Cu_3(\mathbf{1})(\mathbf{2a})(\mathbf{5})]^{3+}$	$<10^{-4}$	0	0

in presence of **6**, **7** (10 equiv. each with respect to Cu^{+}) *via* ^{1}H NMR analysis. Then, step-by-step, single inputs of **3**, **4**, and Fe^{2+} were added to furnish **SIIa**, **SIIIa** and **SIa**. The whole cycle was performed twice (Table 2). The starting state, **SIa** generated 33% of **8** in first cycle and 30% in the second cycle. Likewise, **SIIa** furnished 13% and 8%. The decreased yield in the 2nd cycle may be attributed to increased product inhibition. In contrast, in **SIIIa**, no catalytic activity was observed. As imine **5** blocks one of the copper(I) phenanthroline units, the biped **2a** is unable to depart from the other two sites. By adding iron(II), **SIa** was regained and catalytic activity reignited (Table 2). Thus, a catalytic machinery is presented that changes its catalytic activity through "control and adaptability".

In conclusion, by feeding the catalytic machinery with molecular brakestones, one can control both motional speed and catalytic activity in a stepwise and reversible manner from fully ON to OFF.

We thank the DFG (Schm 647/20-2 and Schm 647/22-1, No 491092614) and the Univ. of Siegen for continued support.

Conflicts of interest

There are no conflicts to declare.

Notes and references

1 (*a*) E. Whitehead, The regulation of enzyme activity and allosteric transition, *Prog. Biophys. Mol. Biol.*, 1970, **21**, 321–397; (*b*) G. G. Hammes, Multiple conformational changes in enzyme catalysis, *Biochemistry*, 2002, **41**, 8221–8228; (*c*) I. Zoi, J. Suarez, D. Antoniou, S. A. Cameron, V. L. Schramm and S. D. Schwartz, Modulating Enzyme Catalysis through Mutations Designed to Alter Rapid Protein Dynamics, *J. Am. Chem. Soc.*, 2016, **138**, 3403–3409.

2 (*a*) D. A. Leigh, V. Marcos and M. R. Wilson, Rotaxane Catalysts, *ACS Catal.*, 2014, **4**, 4490–4497; (*b*) M. Schmittel, From self-sorted coordination libraries to networking nanoswitches for catalysis, *Chem. Commun.*, 2015, **51**, 14956–14968; (*c*) J. Choudhury, Recent developments on artificial switchable catalysis, *Tetrahedron Lett.*, 2018, **59**, 487–495; (*d*) L. van Dijk, M. J. Tilby, R. Szpera, O. A. Smith, H. A. P. Bunce and S. P. Fletcher, Molecular machines for catalysis, *Nat. Rev. Chem.*, 2018, **2**, 117.

3 (*a*) M. Schmittel, S. De and S. Pramanik, Reversible ON/OFF nanoswitch for organocatalysis: mimicking the locking and unlocking operation of CaMKII, *Angew. Chem., Int. Ed.*, 2012, **51**, 3832–3836; (*b*) V. Blanco, A. Carlone, K. D. Hänni, D. A. Leigh and B. Lewandowski, A Rotaxane-Based Switchable Organocatalyst, *Angew. Chem., Int. Ed.*, 2012, **51**, 5166–5169; (*c*) V. Blanco, D. A. Leigh, V. Marcos, J. A. Morales-Serna and A. L. Nussbaumer, A Switchable [2]Rotaxane Asymmetric Organocatalyst That Utilizes an Acyclic Chiral Secondary Amine, *J. Am. Chem. Soc.*, 2014, **136**, 4905–4908; (*d*) S. Gaikwad, A. Goswami, S. De and M. Schmittel, A Metalloregulated Four-State Nanoswitch Controls Two-Step Sequential Catalysis in an Eleven-Component System, *Angew. Chem., Int. Ed.*, 2016, **55**, 10512–10517.

4 Some early key papers:(*a*) F. Würthner and J. Rebek, Light-Switchable Catalysis in Synthetic Receptors, *Angew. Chem., Int. Ed. Engl.*, 1995, **34**, 446–448; (*b*) R. Cacciapaglia, S. Di Stefano and L. Mandolini, The Bis-Barium Complex of a Butterfly Crown Ether as a Phototunable Supramolecular Catalyst, *J. Am. Chem. Soc.*, 2003, **125**, 2224–2227; (*c*) J. Wang and B. L. Feringa, Dynamic control of chiral space in a catalytic asymmetric reaction using a molecular motor, *Science*, 2011, **331**, 1429–1432.

5 (*a*) Some recent papers:P. Bora, S. Jakkampudi, R. Parella, N. Sakkani, Q. Dai, M. Bihani, H. D. Arman and J. C.-G. Zhao, Diastereodivergent synthesis of 4-oxocyclohexanecarbaldehydes by using the modularly designed organocatalysts upon switching on their iminium catalysis, *Chem. Commun.*, 2021, **57**, 5334–5337; (*b*) K. Nakamura, M. Kondo, C. G. Krishnan, S. Takizawa and H. Sasai, Azopyridine-based chiral oxazolines with rare-earth metals for photoswitchable catalysis, *Chem. Commun.*, 2021, **57**, 7414–7417.

6 M. Schmittel and P. Howlader, Toward Molecular Cybernetics - the Art of Communicating Chemical Systems, *Chem. Rec.*, 2021, **21**, 523–543.

7 G. Ashkenasy, T. M. Hermans, S. Otto and A. F. Taylor, Systems chemistry, *Chem. Soc. Rev.*, 2017, **46**, 2543–2554.

8 P. K. Biswas, S. Saha, T. Paululat and M. Schmittel, Rotating Catalysts Are Superior: Suppressing Product Inhibition by Anchimeric Assistance in Four-Component Catalytic Machinery, *J. Am. Chem. Soc.*, 2018, **140**, 9038–9041.

9 I. Paul, A. Goswami, N. Mittal and M. Schmittel, Catalytic Three-Component Machinery: Control of Catalytic Activity by Machine Speed, *Angew. Chem., Int. Ed.*, 2018, **57**, 354–358.

10 (*a*) Z. He, W. Jiang and C. A. Schalley, Integrative self-sorting: a versatile strategy for the construction of complex supramolecular architecture, *Chem. Soc. Rev.*, 2015, **44**, 779–789; (*b*) M. L. Saha and M. Schmittel, Degree of molecular self-sorting in multicomponent systems, *Org. Biomol. Chem.*, 2012, **10**, 4651–4684; (*c*) W. Jiang and C. A. Schalley, Integrative self-sorting is a programming language for high level self-assembly, *Proc. Natl. Acad. Sci. U. S. A.*, 2009, **106**, 10425–10429.

11 S. Saha, P. K. Biswas, I. Paul and M. Schmittel, Selective and reversible interconversion of nanosliders commanded by remote control via metal-ion signaling, *Chem. Commun.*, 2019, **55**, 14733–14736.

12 A. Ghosh, I. Paul and M. Schmittel, Cooperative Effects in Switchable Catalysis, *Angew. Chem., Int. Ed.*, 2021, **60**, 20558–20562.

13 N. Mittal, I. Paul, S. Pramanik and M. Schmittel, Remote control of the reversible assembly/disassembly of supramolecular aggregates, *Supramol. Chem.*, 2020, **32**, 133–138.

14 S. Pramanik and I. Aprahamian, Hydrazone Switch-Based Negative Feedback Loop, *J. Am. Chem. Soc.*, 2016, **138**, 15142–15145.

15 M. L. Saha, S. Neogi and M. Schmittel, Dynamic heteroleptic metal-phenanthroline complexes: from structure to function, *Dalton Trans.*, 2014, **43**, 3815–3834.

16 S. K. Samanta and M. Schmittel, Four-Component Supramolecular Nanorotors, *J. Am. Chem. Soc.*, 2013, **135**, 18794–18797.

17 N. Mittal, M. S. Özer and M. Schmittel, Four-Component Catalytic Machinery: Reversible Three-State Control of Organocatalysis by Walking Back and Forth on Track, *Inorg. Chem.*, 2018, **57**, 3579–3586.

18 S. Gaikwad, M. L. Saha, D. Samanta and M. Schmittel, Five-component trigonal nanoprism with six dynamic corners, *Chem. Commun.*, 2017, **53**, 8034–8037.

